



First optical observation of ^{10}B -neutron capture reactions using a boron-added liquid scintillator for quality assurance in boron neutron capture therapy

Akihiro Nohtomi¹ · Hideya Maeda¹ · Naoya Sakamoto¹ · Genichiro Wakabayashi² · Takushi Takata³ · Yoshinori Sakurai³

Received: 15 October 2021 / Accepted: 20 November 2021
© Japanese Society of Radiological Technology and Japan Society of Medical Physics 2021

Abstract

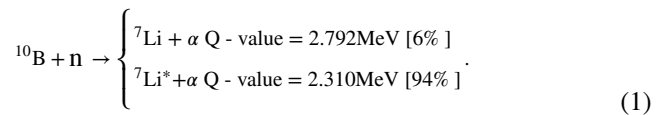
^{10}B -neutron capture was observed optically using a boron-added liquid scintillator. Trimethyl borate was dissolved in a commercially available liquid scintillator at natural boron concentrations of approximately 1 wt% and 0.25 wt%. The boron-added liquid scintillator was placed in a phantom quartz bottle and irradiated by thermal neutrons ($\sim 10^5 \text{ n}/[\text{cm}^2 \text{ s}]$) for 150, 300, and 600 s. The luminescence of the liquid scintillator was clearly observed using a cooled charge-coupled device (CCD) camera during irradiation. The luminance value recorded by the CCD camera was proportional to the duration of irradiation by thermal neutrons. The luminescence distribution showed reasonable agreement with that of energy deposition by Li and alpha particles from ^{10}B -neutron capture reactions calculated via Monte Carlo simulations. When trimethyl borate was not dissolved in the liquid scintillator (0 wt% natural boron), no visible luminescence was observed even after 600 s of irradiation. These findings demonstrate that the observed luminance originates from the Li and alpha particles generated by ^{10}B -neutron capture reactions. Consequently, the luminescence distribution is directly related to the boron dose of the liquid scintillator. To the best of our knowledge, direct experimental optical observations of boron dose distribution have not yet been reported. This novel technique will be useful for quality assurance in boron neutron capture therapy (BNCT) because instantaneous neutron irradiation may be sufficient for the observing the intense neutron beam used in clinical BNCT ($\sim 10^9 \text{ n}/[\text{cm}^2 \text{ s}]$), and quick evaluation of the boron dose distribution is expected to be feasible.

Keywords Boron neutron capture therapy (BNCT) · Liquid scintillator · Charge-coupled device (CCD) camera · Boron dose distribution · Quality assurance (QA)

1 Introduction

Boron neutron capture therapy (BNCT) is a radiation therapy that selectively kills tumor cells through nuclear reactions between boron-10 and neutrons (^{10}B -neutron capture reactions) [1]. Following the $^{10}\text{B}(n,\alpha)^7\text{Li}$ reaction [Eq. (1)],

energetic Li and alpha particles are generated, and a fatal dose is applied only to tumor cells.



The dose deposited by Li and alpha particles is called the boron dose, and it is theoretically proportional to the number of ^{10}B -neutron capture reactions. However, direct measurement of the ^{10}B -neutron capture reaction is practically difficult because of the very short range of Li and alpha particles in tissue, which is typically less than approximately 15 μm . As an alternative method, the measurement of prompt gamma rays (0.478 MeV) from the excited state of the Li particle ($^7\text{Li}^*$) has been proposed; these gamma rays are emitted with 94% probability for a ^{10}B -neutron capture

✉ Akihiro Nohtomi
nohtomi.akihito.858@m.kyushu-u.ac.jp

¹ Graduate School of Medical Sciences, Kyushu University, 3-1-1 Maidashi, Higashi-ku, Fukuoka 812-8582, Japan

² Atomic Energy Research Institute, Kindai University, 3-4-1 Kowakae, Higashiosaka-shi, Osaka 577-8502, Japan

³ Institute for Integrated Radiation and Nuclear Science, Kyoto University, 2 Asashiro-Nishi, Kumatori-cho, Sennan-gun, Osaka 590-0494, Japan

reaction (γ -ray telescope) [2]. However, imaging and detection of these 0.478-MeV gamma rays have not yet been satisfactorily realized owing to technical problems, such as the rejection of the intense gamma-ray background, low detection efficiency of high-energy gamma rays, and insufficient energy and position resolution of currently available gamma-ray detectors [3–6].

Yabe et al. recently measured an optical image of Cerenkov light in water during irradiation by a neutron beam from a BNCT system [7]. Using a cooled charge-coupled device (CCD) camera, they successfully observed water Cerenkov light caused by electrons produced mainly by 2.2-MeV prompt gamma rays from the ^1H -neutron capture reaction, $^1\text{H}(n, \gamma)^2\text{H}$. Although the image observed by Yabe et al. was not a neutron dose distribution but rather an approximate prompt gamma-ray dose distribution, the image represents the results of neutron irradiation of water. The observation technique will be useful for quality assurance (QA) in BNCT because it enables simple, quick evaluation of the neutron information practically.

Motivated by the report of Yabe et al. [7], in this study, we attempted direct optical observation of ^{10}B -neutron capture reactions. Trimethyl borate ($\text{C}_3\text{H}_9\text{BO}_3$) was dissolved in a commercially available liquid scintillator. The luminescence of a phantom quartz bottle filled with a boron-added liquid scintillator was observed using a cooled CCD camera during thermal neutron irradiation. Monte Carlo simulations were performed to compare the calculated boron dose distribution and observed ^{10}B -neutron capture reactions.

2 Materials and methods

2.1 Beam profile measurement of thermal neutrons using the self-activation of a CsI plate

^{10}B -neutron capture reactions were observed optically using thermal neutrons at the E-3 irradiation port facility of the Kyoto University Research Reactor (KUR) [Fig. 1(a)]. The facility was originally developed for the microanalysis of ^{10}B concentration in tissues using a prompt gamma-ray

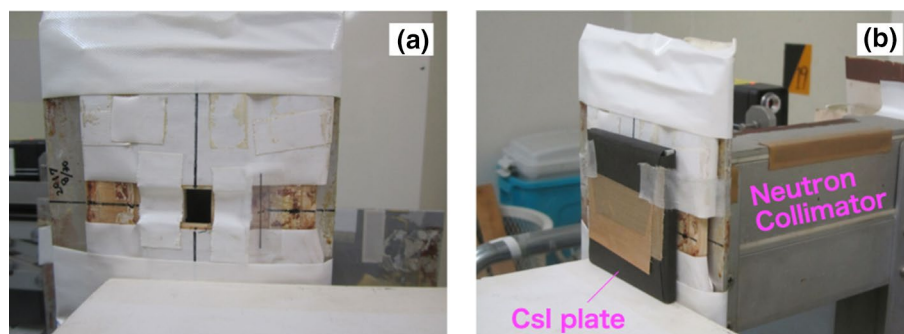
spectrometry system [8]. This system supplies an almost pure thermal neutron beam from the nuclear reactor core through a long neutron duct and has very low background gamma-ray contamination for (n, γ) measurements. The gamma-ray background was less than 1 mSv/h at the exit of the irradiation port. The E-3 irradiation port facility is described in detail in [8].

Before the optical observations of ^{10}B -neutron capture reactions, the beam profile of thermal neutrons was measured at the E-3 irradiation port facility using the self-activation of a CsI scintillator plate. The E-3 irradiation port was originally designed to obtain a parallel thermal neutron beam using a long neutron collimator. However, the beam profile has not yet been precisely measured. The beam profile at the exit of the collimator was evaluated to confirm the shape of the beam profile precisely. After thermal neutron irradiation of the CsI plate, the neutron intensity distribution on the plate was observed using a cooled CCD camera and analyzed using decaying self-activation imaging [9, 10]. This technique, which our group recently proposed, is based on the analysis of the time variation of the radioactivity of certain generated species that remained inside the CsI plate after neutron irradiation was stopped. In this measurement, the radioactivity of ^{128}I generated by the neutron capture reaction in CsI was assessed for imaging using this technique.

A CsI plate (75 mm \times 75 mm \times 2 mm), which was packed into an aluminum container with a quartz (SiO_2) window, was irradiated at the exit of the collimator at the E-3 irradiation port facility, as shown in Fig. 1(b). The plate was covered with thick black paper during neutron irradiation for ambient light shielding. After 75 min of irradiation, the luminescence distributions on the CsI plate were recorded every 1 min as a series of images using a cooled CCD camera (SBIG, STF8300M) operating at -5°C with a telescope lens (SIGMA, 30 mm F1.4 DC) in a black box for 1,000 min.

A gold foil disk with a diameter of 10 mm was irradiated to evaluate the thermal neutron fluence rate at the same

Fig. 1 **a** Exit window of neutrons at the E-3 port facility. **b** Neutron irradiation of CsI plate for beam profile measurement



position using the conventional activation analysis method [11].

2.2 Optical observations of ^{10}B -neutron capture reactions using boron-added liquid scintillator

To observe the distribution of the ^{10}B -neutron capture reactions, we used a liquid scintillator and a cooled CCD camera. Trimethyl borate ($\text{C}_3\text{H}_9\text{BO}_3$) was dissolved in a commercially available liquid scintillator (InstaGel Plus, PerkinElmer Co., Ltd.) to obtain natural boron concentrations of approximately 1 wt% and 0.25 wt%. The natural abundance ratio of ^{10}B is 20%. The main component of the liquid scintillator (InstaGel Plus) is pseudocumene (C_9H_{12}). Both trimethyl borate and pseudocumene are transparent liquids at room temperature, and trimethyl borate is well soluble in pseudocumene.

The boron-added liquid scintillator was placed into phantom quartz (SiO_2) bottle with an inner square cross-section of 10 mm \times 10 mm and a full volume capacity of approximately 4.5 cm^3 . A single liquid scintillator was also placed in a phantom quartz bottle (0 wt% natural boron) for comparison with the boron-added liquid scintillator. The height from the bottom of the bottle to its shoulder is approximately 35 mm, as shown in Fig. 2(a). We chose a quartz bottle and rather than a typical borosilicate glass bottle because the latter has a non-negligible B_2O_3 content (typically 13 wt%). The phantom quartz bottle in a black box was irradiated with collimated thermal neutrons from the E-3 port, as shown in Fig. 2(b). The distance from the exit window to the entrance surface of the bottle was approximately 40 cm. During neutron irradiation, the cover door of the black box, an aluminum plate with a thickness of approximately 3 mm, was closed for ambient light shielding. A schematic of the

experimental setup for the optical observation is shown in Fig. 3.

The phantom quartz bottles were imaged using a cooled CCD camera operating at $-5\text{ }^\circ\text{C}$ (SBIG, STF8300M) with an $f/0.95$ telescope lens (Schneider, Xenon25/F0.95). This cooled CCD camera was also used to measure the beam profile of the thermal neutrons. The distance between the CCD camera and the bottle surface was approximately 32 cm. The built-in CCD element was monochrome with a pixel size of $3,326 \times 2,504$ and depth of 16 bits (Kodak, KAF-8300). The peak sensitivity of the CCD element was 550 nm. To detect weak luminescence, we used a cooled CCD camera with a pixel binning mode of $5\text{ px} \times 5\text{ px}$.

After each image of the liquid scintillator luminescence was obtained, a background image of the phantom was acquired without irradiation by thermal neutrons to correct

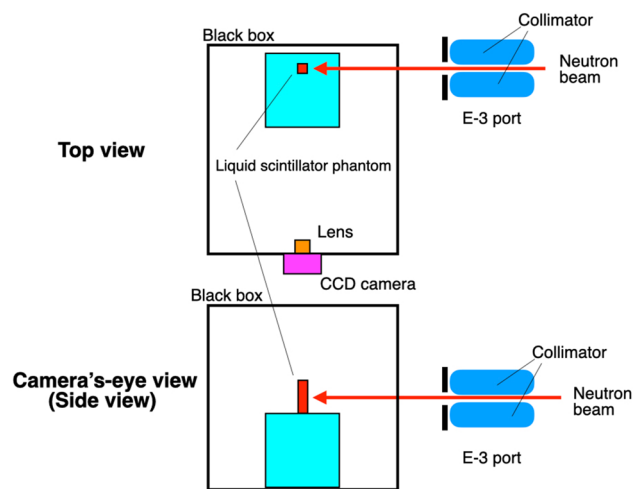
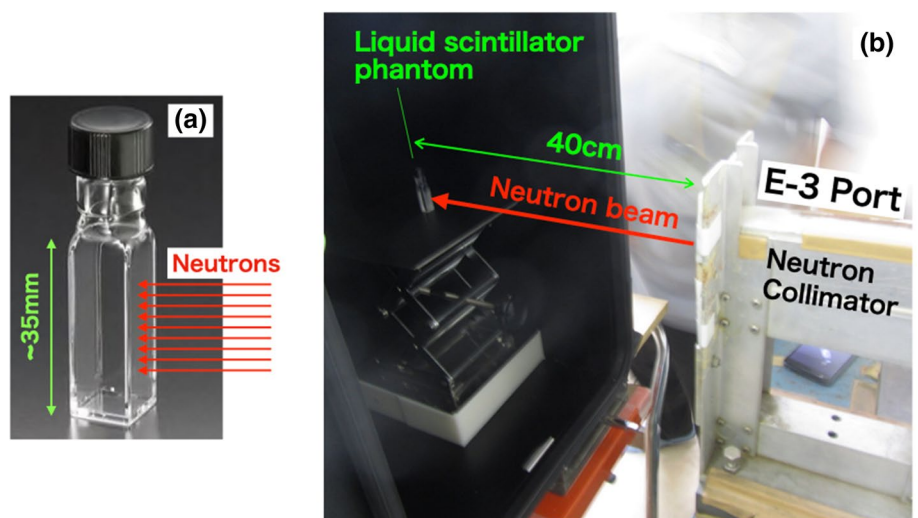


Fig. 3 Diagram of experimental setup for observing luminescence image using CCD camera

Fig. 2 Photographs of a phantom quartz bottle and b experimental setup for neutron irradiation of liquid-scintillator-filled phantom in a black box to observe a luminescence image



for the background and nonuniformity of the CCD camera. The obtained images were processed using the public domain software ImageJ [12]. Apparent noise spots caused by the absorption of scattered neutrons by the CCD camera were first eliminated using the ImageJ function “Remove Outliers,” which uses high-intensity and small-pixel information.

2.3 Monte Carlo simulations

Monte Carlo simulations were performed to calculate the energy deposition (dose) of charged particles and gamma rays (0.478 MeV) from the $^{10}\text{B}(n,\alpha)^7\text{Li}$ and $^{10}\text{B}(n,\alpha\gamma)^7\text{Li}^*$ reactions and gamma rays (2.2 MeV) from the $^1\text{H}(n,\gamma)^2\text{H}$ reaction. We used PHITS code ver. 3.24 [13, 14], to model a phantom quartz bottle filled with a boron-added liquid scintillator. The bottle was placed in a black box and irradiated with collimated parallel monoenergetic thermal neutrons (0.025 eV) from a source of uniform neutron emission, which had vertical and horizontal dimensions of 21 mm and 15 mm, respectively. The neutron source was located outside the black box. The dimensions of the source area were determined based on the beam profile measurements described in Sect. 2.1. The wall of the black box was modeled using aluminum plates with a thickness of 3 mm. Therefore, the neutrons crossed the aluminum plates before reaching the phantom quartz bottle. The energy deposition distributions were calculated using the [t-deposit] tally in the PHITS code for each type of ionizing radiation (charged particles and gamma rays). The elemental composition of the boron-added liquid scintillator (InstaGel Plus) was obtained from PerkinElmer Co., Ltd. [15]. The total number of histories was 10^9 , and the relative statistical uncertainty was less than 2%.

3 Results

3.1 Beam profile of the thermal neutrons

Figure 4 displays an ^{128}I self-luminescence image (beam’s-eye view) observed by the CCD camera. The ^{128}I luminescence component was extracted using decaying self-activation imaging. The yellow rectangle indicates the region at 10% of the maximum luminance, and the horizontal and vertical dimensions are 15 mm and 21 mm, respectively. These values are approximately the same as the physical dimensions of the collimator window. Figure 5 presents the horizontal and vertical beam profiles of the luminescence observed using the CCD camera. The results in Fig. 5 confirm that the thermal neutron beam profile at the E-3 port facility is almost uniform and symmetrical along the vertical direction, with a spreading of approximately 20 mm. By contrast, along the horizontal direction, the beam profile

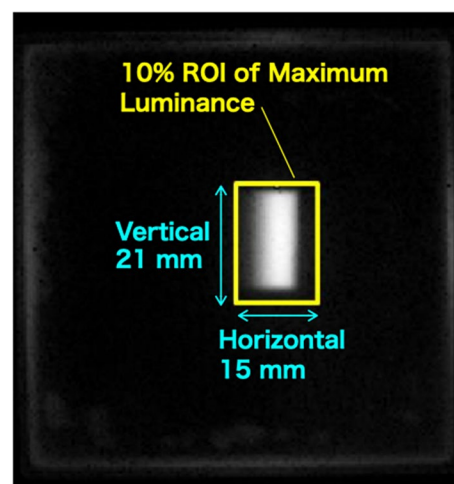


Fig. 4 ^{128}I self-luminescence image (beam’s-eye view) observed by the CCD camera

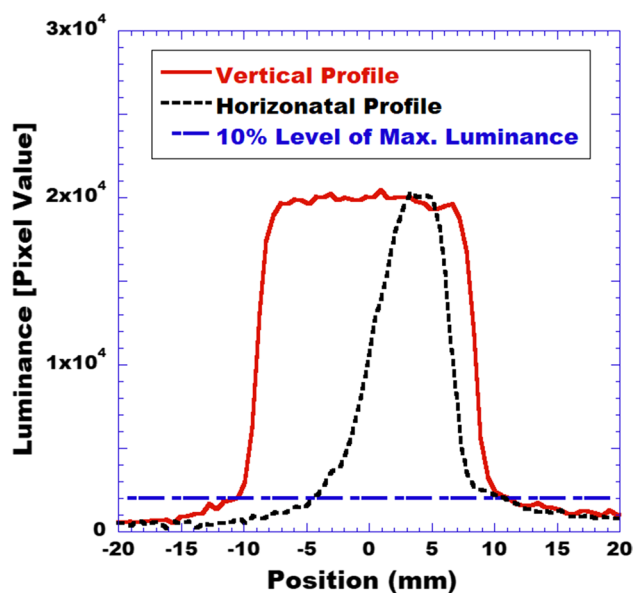


Fig. 5 Horizontal and vertical beam profiles of the luminescence observed by the CCD camera with self-activation by the CsI plate

resembles a distorted Gaussian distribution and does not have a flat region at the top.

The thermal neutron fluence rate at the irradiation port was evaluated to be $1.8 \times 10^5 \text{ n}/[\text{cm}^2 \text{ s}]$ via conventional activation analysis of the gold foil when the thermal output of the KUR was 1 MW.

3.2 Optical observations of ^{10}B -neutron capture reactions using boron-added liquid scintillator

Figure 6 shows luminescence images of the phantom quartz bottle filled with the boron-added liquid scintillator

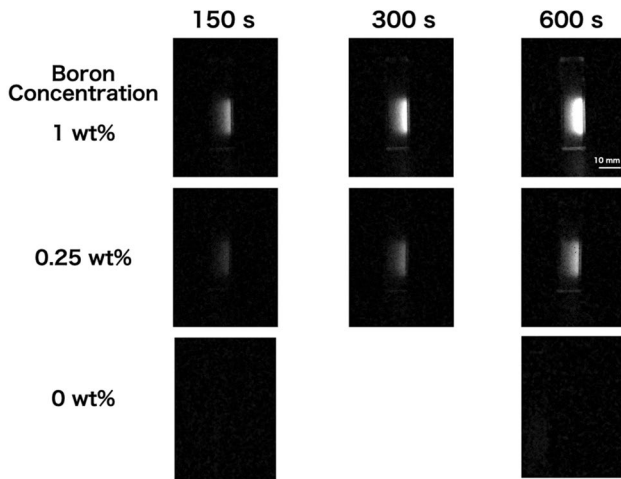


Fig. 6 Luminescence images of boron-added liquid scintillators with different boron concentrations during neutron irradiation for different durations

during thermal neutron irradiation for 150, 300, and 600 s at natural boron concentrations of 1, 0.25, and 0 wt%. The images have the same maximum intensity. In the center of the images of the phantom irradiated by neutrons from the right, a luminescence distribution can be clearly observed covering approximately 20 mm along the vertical direction at the neutron entrance surface for the boron-added liquid scintillators with natural boron concentrations of 1 and 0.25 wt%. The luminescence intensity is typically highest at the neutron-incident surface (right-hand side) and gradually decreases with increasing depth of the neutron beams. The luminescence intensity is higher at the natural boron concentration of 1 wt% than that at the concentration of 0.25 wt% for all irradiation times. In this study, slight luminescence was observed not only in the neutron-irradiated region but also at the bottom of the quartz bottle owing to the effect of light reflected through the inside of the bottle wall. When trimethyl borate was not dissolved in the liquid scintillator (0 wt% natural boron), no visible luminescence was observed even after 600 s of irradiation (Fig. 6).

As shown in Fig. 7, the luminance value of the CCD camera (mean pixel value) evaluated at the center of each luminescent region is generally proportional to the duration of thermal neutron irradiation at both natural boron concentrations of 1 and 0.25 wt%. For the same irradiation time, the luminance at the concentration of 1 wt% was approximately three times that at the concentration of 0.25 wt%. Invisible but very slight luminescence was detected at 0 wt%, which was less than 2% of that at 1 wt% for the same irradiation time.

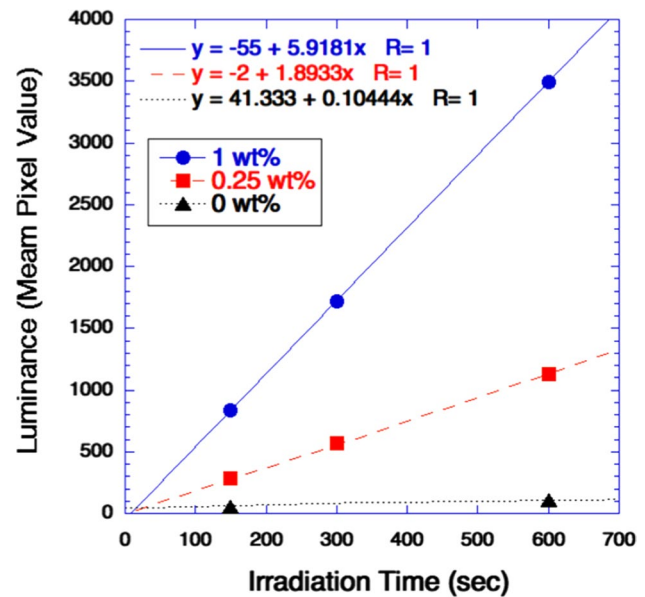


Fig. 7 Luminance of boron-added liquid scintillator as a function of neutron irradiation time

3.3 Comparison of luminescence images with Monte Carlo simulation

Figure 8(a) shows the simulated distribution of the dose deposited by the Li and alpha particles for the boron-added liquid scintillator with the natural boron concentration of 1 wt%. The neutron beam was incident on the right side. Similarly, the distribution of the dose deposited by the gamma rays is shown in Fig. 8(b). The image of the dose distribution deposited by Li and alpha particles in Fig. 8(a) resembles the observed images at the natural boron concentrations of 1 and 0.25 wt% presented in Fig. 6. By contrast, no apparent distribution appears in the image of the dose deposited by the gamma rays, as shown in Fig. 8(b).

The depth profiles (horizontal direction; Fig. 6 (1 wt%, 600 s) and Fig. 8) and lateral profiles (vertical direction; in Fig. 6 (1 wt%, 600 s) and Fig. 8) of the measured and calculated images are presented in Fig. 9(a) and (b), respectively, for comparison; the profiles show the relative intensity distributions.

As demonstrated in Fig. 9(a), the depth profiles of the boron dose based on the measured optical image and the calculated image are nearly identical. The small peak observed for the boron dose at the depth of 0 mm is luminescence from the bottle wall due to light reflection inside the quartz. By contrast, in the lateral profile shown in Fig. 9(b), the boron dose distribution in the measured optical image is narrower than that in the calculated image, and non-negligible discrepancies appear between 5 and 10 mm and -5 and -10 mm. This is because an unrealistically simple neutron source model was used for the calculation. Although

Fig. 8 Dose distributions in liquid scintillator calculated via Monte Carlo simulation for neutron irradiation by **a** Li + alpha particles and **b** gamma rays

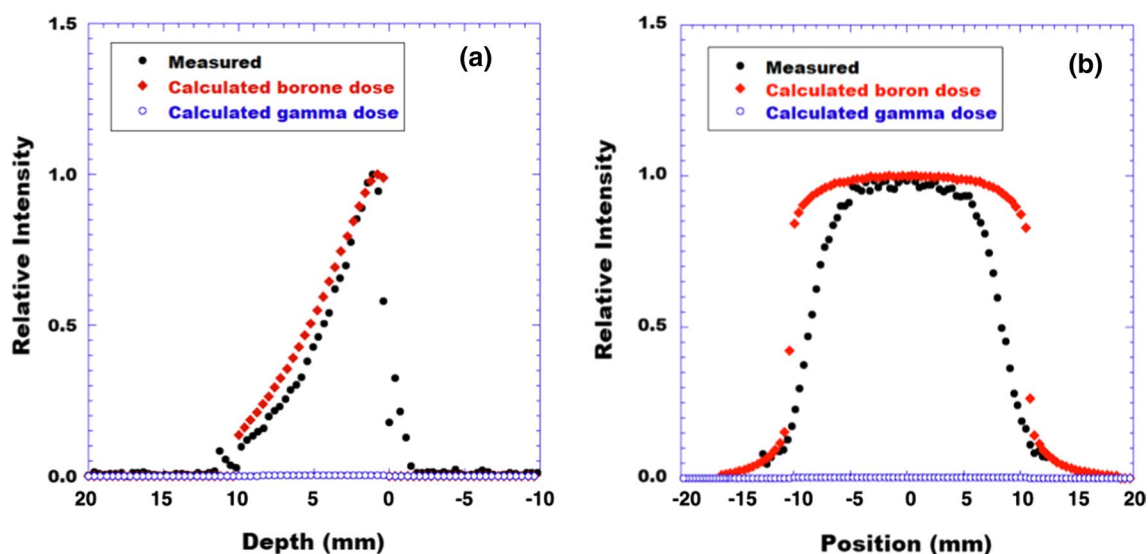
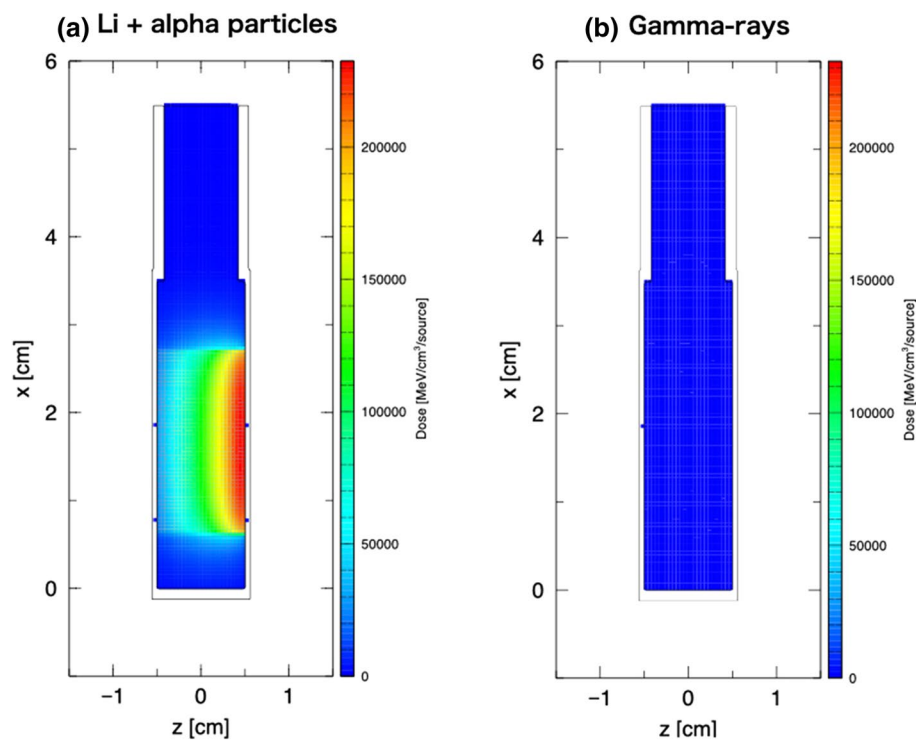


Fig. 9 **a** Depth and **b** lateral profiles of measured luminescence and distribution of dose deposited by Li + alpha particles and gamma rays

an ideal parallel neutron beam emitted from a simple square uniform neutron source was assumed in the Monte Carlo simulation, the actual neutron source might not be reasonably uniform and the neutron beam might broaden to some extent through the penetration of 40 cm of air. As a result, the full width at half maximum of the relative intensity profile became narrower. As displayed in Fig. 5, the measured vertical profile was almost uniform from -10 to 10 mm. Therefore, in the above Monte Carlo calculation, as

an approximation, a simple uniform source was used for the simulation despite the measurement for simplicity. Notably, the vertical luminance profile in Fig. 5 is similar to the measured profile provided in Fig. 9(b).

The relative intensities of both the depth and lateral profiles for the gamma rays are very small. The calculated gamma-ray dose was approximately 0.3% of the maximum Li + alpha dose (boron dose) at the depth of 0 mm, as shown in Fig. 9(a).

When the aluminum plate representing the cover door (3 mm in thickness) was removed from the simulation, the calculated dose distributions were almost unchanged. Therefore, the insertion of the thin aluminum cover plate into the neutron beam path has a negligible effect to the neutron beam profile and intensity.

4 Discussion

The profile measurement of the thermal neutron beam using the self-activation of a CsI plate indicates that the collimated beam had a uniform, symmetrical area with a width of 21 mm along the vertical direction with 10% of the maximum peak height. Therefore, uniform irradiation by thermal neutrons may be expected along the vertical direction with approximately 20 mm of spreading when the liquid scintillator phantom is exposed to the neutron beam and observed using the CCD camera from the side, as shown in Fig. 3. By contrast, along the horizontal direction, the beam profile resembles a distorted Gaussian distribution and does not have a flat region at the top. The reason for this shape distortion is unknown.

The thermal neutron fluence rate at the irradiation port was found to be $1.8 \times 10^5 \text{ n}/[\text{cm}^2 \text{ s}]$ according to conventional activation analysis of the gold foil when the thermal output of the KUR was 1 MW. At the bottle position, the thermal neutron fluence rate was reduced to approximately $1 \times 10^5 \text{ n}/[\text{cm}^2 \text{ s}]$ owing to some broadening through the penetration of 40 cm of air [8]. This thermal neutron intensity is much lower than the typical value for a clinical BNCT system, which is $\sim 10^9 \text{ n}/[\text{cm}^2 \text{ s}]$.

As indicated in Fig. 6, the luminescence of the boron-added liquid scintillator during irradiation by thermal neutrons was clearly observed using the cooled CCD camera. The vertical dimension of the luminescent region was approximately 20 mm at the right entrance surface of the bottle, which is approximately equal to the vertical dimension of the incident neutron beam. The luminance recorded by the CCD camera was generally proportional to the duration of thermal neutron irradiation, as shown in Fig. 7. When trimethyl borate was not dissolved in the liquid scintillator (0 wt% natural boron), no visible luminescence was observed even after 600 s of irradiation (Fig. 6). The luminescence distribution was in reasonable agreement with the distribution of the dose deposited by Li and alpha particles from ^{10}B -neutron capture reactions, calculated via the Monte Carlo simulation, as indicated in Figs. 8(a) and 9. These findings demonstrate that the observed luminance originates from the Li and alpha particles generated by ^{10}B -neutron capture reactions. Consequently, the luminescence distribution is directly related to the boron dose of the liquid scintillator. To the best of our knowledge, direct experimental

optical observations of boron dose distribution have not yet been reported.

The results of the Monte Carlo calculation reveal that the energy deposited by prompt gamma rays (0.478 MeV) from the $^{10}\text{B}(\text{n}, \alpha \gamma)^7\text{Li}^*$ reaction and prompt gamma rays (2.2 MeV) from the $^1\text{H}(\text{n}, \gamma)^2\text{H}$ reaction is approximately less than or equal to 0.3% of the maximum dose deposited by Li and alpha particles from the ^{10}B -neutron capture reaction. The main reason for this is that prompt gamma rays exhibit a much lower linear energy transfer than energetic heavy charged particles. Therefore, the effect of the gamma rays was almost negligible, and no visible luminescence was observed when trimethyl borate was not dissolved in the liquid scintillator even after 600 s of irradiation (Fig. 6).

As in Fig. 7, the luminance values of the boron-added liquid scintillator with the natural boron concentration of 1 wt% are approximately three times those of the scintillator with the concentration of 0.25 wt% for the same irradiation time. If the luminescence is primarily proportional to the boron-10 concentration, then the luminescence at the natural boron concentration of 1 wt% should be four times that at the concentration of 0.25 wt%. This discrepancy may be due to chemical quenching of the liquid scintillator by excess trimethyl borate, which reduces the luminescence intensity due to the ^{10}B -neutron capture reactions. Notably, this quenching effect occurs equally for all ^{10}B -neutron capture reactions at a certain boron concentration because the emitted Li and alpha particles have constant energies determined by the Q value of the nuclear reaction.

As in Fig. 9(a), around the surface depth from -2 to 0 mm, the measurement is higher than the calculated boron dose (relative intensity ~ 0). As mentioned in Results, the discrepancy may arise from the luminescence from the bottle wall due to light reflection inside the quartz, which was not included in the calculation.

The technique proposed in this work using a boron-added liquid scintillator and a CCD camera will be useful for QA in BNCT because instantaneous neutron irradiation may be sufficient for observation of the intense neutron beam used in clinical BNCT ($\sim 10^9 \text{ n}/[\text{cm}^2 \text{ s}]$), even at a lower boron concentration. A quick evaluation of the boron dose distribution is feasible if the CCD camera has a good position resolution. Since this liquid scintillator comprises organic matter, it can be assumed to be essentially tissue-equivalent, which is also advantageous for dosimetry.

5 Conclusions

^{10}B -neutron capture reactions were successfully observed optically for the first time using a boron-added liquid scintillator and cooled CCD camera. By comparing the observed luminescence image with that calculated through Monte

Carlo simulations, we confirmed that the luminescence distribution of ^{10}B -neutron capture reactions is equivalent to the boron dose of the liquid scintillator. Consequently, the boron dose originating from ^{10}B -neutron capture reactions can be measured directly using the proposed technique quickly and precisely for QA in BNCT. We plan to experimentally verify the technique using a clinical BNCT system; the results will be presented in the near future.

Acknowledgements This work was performed under the Collaboration Research supported by the Institute for Integrated Radiation and Nuclear Science, Kyoto University. This work was partially supported by JSPS KAKENHI grant number JP19K08202. The authors are deeply thankful to Ms. Yui Kanzaki of Kyushu University Hospital for her help with the analysis of the CCD camera image data.

Declarations

Conflict of interest The authors declare that they have no conflict of interest.

Ethical approval This article does not include any studies with human participants or animals.

References

- Locher GL. Biological effects and therapeutic possibilities of neutrons. *Am J Roentgenol Radium Therapy*. 1936;36:1–13.
- Verbakel WFAR, Stecher-Rasmussen F. A g-ray telescope for on-line measurements of low boron concentrations in a head phantom for BNCT. *Nucl Instrum Methods Phys Res Sect A*. 1997;394:163–72.
- Kobayashi T, Sakurai Y, Ishikawa M. A noninvasive dose estimation system for clinical BNCT based on PG-SPECT – Conceptual study and fundamental experiments using HPGe and CdTe semiconductor detectors. *Med Phys*. 2000;27:2124–32.
- Verbakel WFAR, Stecher-Rasmussen F. On-line reconstruction of low boron concentrations by *in vivo* g-ray spectroscopy for BNCT. *Phys Med Biol*. 2001;46:687–701.
- Minsky DM, Valda AA, Kreiner AJ, Green S, Wojnecki C, Ghani Z. First tomographic image of neutron capture rate in a BNCT facility. *Appl Radiat Isot*. 2011;69:1858–61.
- Katabuchi T, Hales B, Hayashizaki N, Igashira M, Khan Z, Kobayashi T, Matsuhashi T, Miyazaki K, Ogawa K, Terada K. Feasibility study on pinhole camera system for online dosimetry in boron neutron capture therapy. *Appl Radiat Isot*. 2014;88:139–42.
- Yabe T, Yamamoto S, Hu N, Kanai Y, Tanaka H, Ono K. First measured optical image of Cerenkov-light in water during irradiation of neutron beam from boron neutron capture therapy (BNCT) system. *Radiat Meas*. 2021;146:106633.
- Kobayashi T, Kanda K. Microanalysis system of ppm-order ^{10}B concentrations in tissue for neutron capture therapy by prompt gamma ray spectrometry. *Nucl Instrum Methods Phys Res*. 1983;204:525–31.
- Nohtomi A, Kurihara R, Kinoshita H, Honda S, Tokunaga M, Uno H, Shinsho K, Wakabayashi G, Koba Y, Fukunaga J, Umezu Y, Nakamura Y, Ohga S. An application of CCD read-out technique to neutron distribution measurement using the self-activation method with a CsI scintillator plate. *Nucl Instrum Methods Phys Res Sect A*. 2016;832:21–3.
- Nohtomi A, Tokunaga M, Wakabayashi G, Shinsho K. Neutron distribution measurement by the self-activation of a CsI plate with CCD Camera using a decaying self-activation imaging technique. Proceedings of the second international symposium on radiation detectors and their uses 2019. Proceedings of the 24: 011041; JPS conference
- Knoll GF. Radiation detection and measurement, 4th edition, p. 767, John Wiley and Sons Inc. (2010).
- Web-site of “ImageJ”: <https://imagej.nih.gov/ij/> (2021/10/1).
- Sato T, Iwamoto Y, Hashimoto S, Ogawa T, Furuta T, Abe S, Kai T, Ratliff HN, Matsuda N, Iwase H, Shigyo N, Sihver L, Niita K. Features of particle and heavy ion transport code system (PHITS) version 3.02. *J Nucl Sci Technol*. 2018;55:684–90.
- Furuta T, Sato T. Medical application of particle and heavy ion transport code system PHITS. *Radiol Phys Technol*. 2021;14:215–25.
- Web-site of “InstaGel Plus, PerkinElmer Co., Ltd.”: https://resources.perkinelmer.com/lab-solutions/resources/docs/APP_LSCCOcktailsElementalComposition.pdf (2021/10/1).

Publisher's Note Springer Nature remains neutral with regard to jurisdictional claims in published maps and institutional affiliations.